ELSEVIER

Nuclear Instruments and Methods in Physics Research A 453 (2000) 103–108

NUCLEAR INSTRUMENTS & METHODS IN PHYSICS RESEARCH Section A

www.elsevier.nl/locate/nima

The HERA-B vertex detector system

C. Bauer[a], M. Bräuer[a], T. Glebe[a], W. Hofmann[a], T. Jagla[a], F. Klefenz[a], K.T. Knöpfle[a,*], V. Pugatch[a], M. Schmelling[a], B. Schwingenheuer[a], E. Sexauer[a], U. Trunk[a], R. Wanke[a], F. Zurheide[a], I. Abt[b], M. Dressel[b], I. Kisel[b], S. Masciocchi[b], B. Moshous[b], T. Perschke[b], M. Sang[b], S. Schaller[b], W. Wagner[b]

[a]*Max-Planck-Institut für Kernphysik, Postfach 103980, D-69029 Heidelberg, Germany*
[b]*Max-Planck-Institut für Physik, Föhringer Ring 8, D-80805 München, Germany*

Accepted 19 June 2000

Abstract

The HERA-B experiment is being built to measure CP violation in the B-system using internal targets at the HERA proton storage ring at DESY. This paper presents an overview of its vertex detector which – apart from an additional superlayer – is realized by a system of 20 Roman pots containing seven superlayers of double-sided silicon microstrip detectors that are operated at 10 mm distance from the proton beam in a high-radiation environment. © 2000 Published by Elsevier Science B.V. All rights reserved.

Keywords: HERA-B; Vertex detector; Roman pot; RF-shield; Silicon microstrip detector; Front-end electronics; Radiation damage

1. Introduction

HERA-B [1] is a fixed target experiment at the HERA proton storage ring of DESY, Hamburg, which aims to measure CP violation in rare B-meson decays. The decay products are detected, momentum-analyzed and identified in a multiparticle spectrometer with a forward acceptance from 10 to 250 mrad in the bending plane. The design is optimized for an efficient study of the 'golden' decay channel $B^0 \to J/\Psi K^0_S$. The B-mesons are produced by interactions of 920 GeV/c protons with eight internal target wires. At $\sqrt{s} \approx 40$ GeV, about 10^6 interactions yield one $b\bar{b}$ pair, and thus the experiment must run with four interactions on average per 96 ns bunch crossing to produce a sufficient number of B-mesons. The corresponding interaction rate of 40 MHz creates a high-radiation environment with a flux similar to that expected at the LHC: (30 MHz · cm^2)/r^2 minimum ionizing particles per cm^2, where r is the radial distance to the beam.

The Vertex Detector System (VDS) [2,3] provides the information for reconstructing the J/Ψ decay vertices and the impact parameters of the tagging particles; in addition, it serves to suppress charm background at the second trigger level. Due to space limitations, the following overview will refer also to figures shown at the conference which are accessible via the world-wide web [4].

2. General layout and mechanics

The VDS consists of 64 double-sided (d.s.) silicon microstrip detectors which are arranged in eight

* Corresponding author.
E-mail address: ktkno@mpi-hd.mpg.de (K.T. Knöpfle).

0168-9002/00/$ - see front matter
PII: S0168-9002(00)00614-8

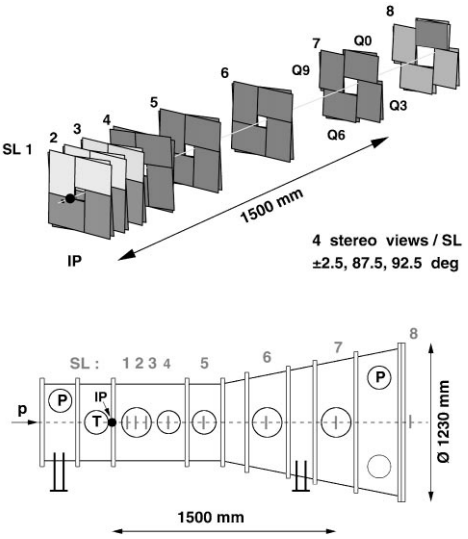

Fig. 1. The arrangement of the 64 silicon detectors in eight superlayers around the beam axis (top), and a schematic side view of the vertex vessel (below). For one quadrant, the flanges (circles) are shown, through which the Roman pots of superlayers 1–7 are inserted. Flanges for pumps and the target stations are labeled by 'P' and 'T', respectively.

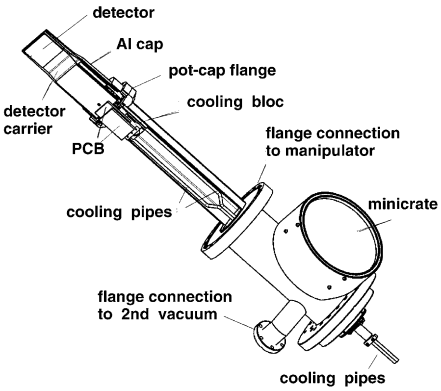

Fig. 2. Layout of the Roman pot for one quadrant of superlayer 5. The overall length is about 940 mm.

superlayers (SLs) of four quadrants around the proton beam axis (Fig. 1), covering an angular range from 10 to 250 mrad and providing four stereo views of $\pm 2.5^\circ$ and $90 \pm 2.5^\circ$. To minimize multiple scattering, the first seven SLs are realized as a Roman pot system that is contained in a 2.6 m long stainless-steel ultra-high vacuum (UHV) vessel; the eighth SL is mounted at 2 m distance from the targets, immediately after the vessel's 3 mm thick aluminium exit window (Fig. 1, bottom).

The detector modules of each quadrant of a SL are housed in a Roman pot that is connected to the vessel via UHV manipulators for both radial and lateral positioning. The radial distance of the detectors from the beam is 10 mm. The detectors are retracted by the same amount during injection. The lateral movement allows the rotation of the detector positions in order to distribute the radiation load over a larger detector area. A view of a Roman pot for SL 5 is shown in Fig. 2. The main support structure is provided by a rather massive steel tube with several flanges that connect to the manipulator and to the secondary vacuum system or carry the feed-through flanges for the cooling pipes and for the electrical lines as well as the minicrate (see below). The two d.s. detectors are mounted back-to-back on top of the pot and are separated by a 150 μm thick aluminium cap from the storage ring vacuum. All parts above the manipulator flange are located within the ring vacuum, and all parts above the pot-cap flange are within the HERA-B acceptance. In consequence, both the cooling block and the cooling pipe – all made from copper – are located outside the detector acceptance.

The support structure for a detector [4, p. 12] consists of a carrier with a fork-like shape underneath the detector and one carrier each for the p- and n-side hybrids and readout chips, respectively. To reduce the radiation load, the readout chips are placed 40 mm away from the detector at larger radial distance; the detector signals are carried to the readout chips by multilayer Kapton cables of 41 μm pitch. The carrier plates are connected to the cooling block and also serve as separate heat sinks for detector and chips. The lengths of the detector carriers and their caps increase from 150 mm in the first SL to 430 mm in the last. The carriers are made of composite materials which have radiation lengths similar to that of carbon. The first consists mainly of an ultra-high-modulus pitch fiber (K1100X), and the second is mainly thermal pyrolytic graphite. They exhibit directional thermal conductivities of 470 and 1270 W/(m K), respectively. With the cooling block at 0°C, temperatures of

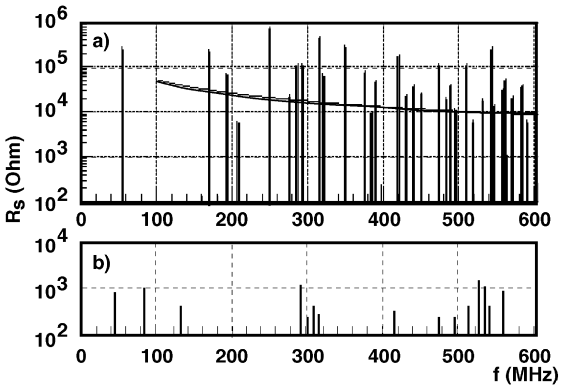

Fig. 3. Results from MAFIA simulations for the multi-resonant shunt impedances R_s of (a) the bare vessel and (b) the vessel with a RF-shield consisting of four steel strips. The curve in the upper part represents the limit of allowed R_s values.

typically 10°C and 30°C are measured at the detector and the readout chips, respectively.

2.1. RF-shielding

Without shielding, the HERA proton beam would excite strong wake-fields inside the cavity-like VDS vessel that could cause beam instabilities in the storage ring as well as heating of installed detector components. Full MAFIA-32 3D simulations [5] show that, without wake-field suppression, several vessel modes exhibit shunt impedances R_s well above the tolerable limit of $R_s < (52\ \mathrm{MHz}/f)100\ \mathrm{k}\Omega$ for frequencies f between 100 and 600 MHz (Fig. 3a). So far, three different shielding options have been tested in the VDS vessel, all of which aim at conducting the mirror current within the vessel by a very low-mass conductive assembly mounted between the beam and the detector modules: (i) a thin Al tube of 44 mm diameter with slots for inserting the detector modules, (ii) eight CuBe wires of 125 μm diameter and (iii) four 5 μm thick and 12.7 mm wide stainless-steel ribbons [4, p. 6]. All options provided sufficient shielding, in agreement with the results from simulations, indicating a reduction of the shunt impedances R_s by two orders of magnitude, or more (Fig. 3b). Since 1997, steel ribbons have been used because of their robustness and low material budget. They extend over the length of almost 2 m from the targets to the exit window, and their distance to the beam axis is adjustable between $r = 22$ mm (for injection) and $r = 7$ mm (for running) by coupling their radial movements to those of the Roman pots in SL 1 and 6. With the bands widely separated, the present setup shows evidence of resonant RF-leakage at certain sharp pot positions. This manifests itself by an increased power loss in the vessel and an associated rise in the vacuum pressure [4, p. 8]. Thus, it remains to be seen if a further reduction of the shielding material, by using fewer or narrower strips, will be feasible.

3. Detectors and electronics readout

Produced by Sintef and HLL Pasing, the d.s. silicon sensors [6] are made from 280 μm thick n-type material with p^+ strips on the junction side and orthogonal n^+ strips on the ohmic side. The n-side strips are insulated either by p^+ blocking implants or by a p-spray layer. Within the sensitive area of $50 \times 70\ \mathrm{mm}^2$, the strip pattern is rotated by 2.5° w.r.t. the wafer edges. The p- and n-sides have 1024 and 1280 readout strips, respectively, at a pitch of about 50 μm. The detectors are AC coupled, have polysilicon bias resistors and multi-guard ring structures developed by HLL Pasing [7]. Non-irradiated detectors hold bias voltages well beyond 200 V at bulk currents of less than 10 μA; the guard ring currents are about 10 times lower. The radiation tolerance has been studied with single-sided p-on-n detectors of equivalent design by simulating the highly non-uniform fluence distribution at HERA-B with 21 MeV protons Coulomb-scattered from a Au-foil. The test results [8] indicate acceptable detector performance up to the expected maximum fluence of 3×10^{14} MIPS/cm^2 for one year, after which the detectors are planned to be exchanged: The irradiated detectors can be operated at bias voltages beyond 500 V and in contrast to punch-through biased devices, the increase of noise is consistent with the increase of the bulk leakage current. Operated at 8°C, regions of maximum and low (10^{12} MIPS/cm^2) fluences exhibit a clear separation of signal (S) and noise (N) at S/N values of 14 and 22, respectively. In particular, full functionality

has been verified throughout the complete sensitive area which contains regions of very different doping concentrations due to the simultaneous existence of original n-type, compensated and type-inverted material.

Front-end processing of the detector signals is performed by the HELIX128-2.2 pipelined analog readout chips mounted on alumina hybrids, one for each detector side, that distribute signals and power. These chips are designed along the RD20 architecture [9], and fabricated in the AMS 0.8 μm bulk CMOS process. On a die size of 14.4×6.2 mm^2, one HELIX128 chip integrates 128 channels, each consisting of a charge sensitive preamplifier, a shaper with 50 ns peaking time, and a 141 cell deep capacitor row as pipeline; the stored charges can be read out sequentially without dead time via an analog multiplexer. Write/read frequencies are 10 and up to 40 MHz, respectively. Operated at 10 cm from the beam, the chips will be exposed to an annual dose of about 1 kGy. This moderate level of radiation tolerance is achieved by biasing the HELIX circuits with constant currents rather than fixed voltages, which compensates the radiation-induced threshold voltage shifts. Irradiations with a ^{137}Cs source show the chips to be still operational after a dose of 5.2 kGy [10,11]. For the unirradiated chip, the equivalent noise charge is $338\ e^- + 38.4\ e^-$/pF; after 1 kGy, the noise offset and slope have increased by about 50% and 33%, respectively. The power consumption of 1.8 mW/channel increases by 14.4%/kGy which allows easy monitoring of the dose deposited in the chips.

Kapton cables (within the acceptance) followed by coaxial cables of a total length of 1.3 m connect the four hybrids in a Roman pot to the outside world; a ring-shaped 4-layer PCB with O-ring seals on both surfaces represents an economical and reliable high-density vacuum feed-through with 108 lines in total. A 'minicrate' mounted directly on top of the feedthrough flange serves to distribute the differential digital control signals (DCS) and the power to the hybrids; it also houses the LEDs (1A194) and driver circuits for the analog optical data transmission. Pairs of chips are read out in daisy-chain mode and connected via 18 large diameter (200 μm) fibers to the electronics hut 50 m away. The use of d.s. detectors requires the readout to be at high potential on at least one side and, to take advantage of a system that is completely decoupled from ground, the supply subsystems are built from fully floating units for all hybrids. Thus, individual continous-type floating voltage regulators whose grounds are connected to the respective terminals of the floating bias voltage supplies (0–600 V, 2 mA, 1 mV ripple) deliver the power for the 8 (10) Helix chips on the p(n)-side hybrids ($\pm$ 2 V, 1 A) and for the associated electronics on the 'minicrate' ($\pm$ 5 V, 1 A). The potential shift for the DCS is provided by coupling capacitors at the input to the 'minicrate'. These signals are generated in the electronics hut and transmitted optically to a fanout 15 m from the vessel. All power supplies are also located there, so that there is no galvanic connection between the front-end readout system and the electronics hut.

At the electronics hut, optical receivers with SFH 250 V pin-diodes convert the signals back into electrical signals and send them for digitization to the front-end driver modules (FEDs). A FED houses 12 channels of 10 bit FADCs which operate at up to 40 MHz. The most significant 8 bits of the FADCs are buffered in the FED and subsequently transmitted into the memory of the second-level buffers (SLBs). From these SLBs, the data is sent on request to the second-level trigger processors and event building. At 20 MHz readout frequency, all 147,456 channels of the VDS are read out, digitized and stored within less than 15 μs.

4. Status and performance

The VDS has been operated with partial instrumentation since 1996 [3]. No failures of its complex auxiliary systems, including the critical two vacuum systems, have occurred so far, and the RF-shielding within the VDS vessel was effective enough to cope with the impressive steady increase of the annual integrated HERA luminosity. At the end of 1998, the optimization process for detector modules and readout chips was concluded, and in 1999 almost 75% of the system was instrumented (see shaded quadrants of Fig. 1). Since January 2000, all the seven SLs of the Roman pot system have been completely installed. The d.s. detectors in

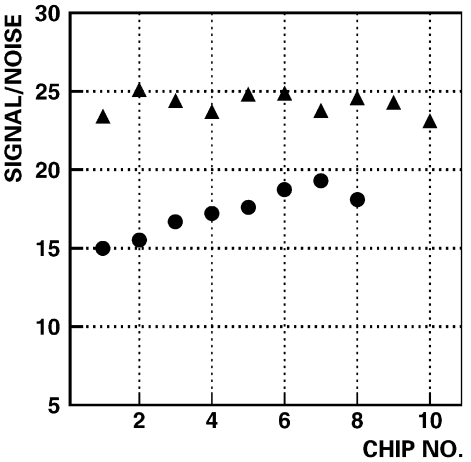

Fig. 4. Chipwise S/N ratios for the p-side (dots) and n-side (triangles) of a d.s. detector module.

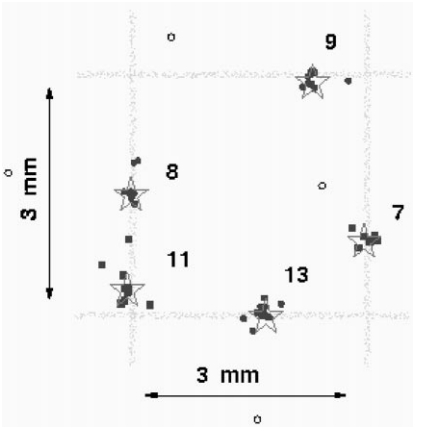

Fig. 5. An event with five primary interaction vertices distributed on four target wires. The total number of reconstructed tracks is 65; the numbers of tracks contributing to each vertex are indicated.

the first three SLs, however, are paired with single-sided modules.

In parallel to the hardware implementation, extensive software has been developed for raw-data processing including cluster finding and sparsification, for track reconstruction and vertexing, for the alignment of the 32 individual pairs of detector wafers, and for the monitoring of data quality. All this code is designed to run on-line.

The results obtained so far indicate that the VDS fulfils the required specifications. Fig. 4 shows the S/N ratios for each chip of a typical d.s. detector module as measured in a recent run. For the n-side, the values are well above 20; for the p-side, they vary systematically from 15 to 20 reflecting the increased and varying capacitive load for the chips which is due to the significantly longer and varied traces on the Kapton cable. With these S/N values, single-hit efficiencies between 97% and 99% have been determined; tracking studies allow the estimation of the noise hit probability to be lower than 0.1%. For stand-alone track reconstruction, two codes have been developed which are based either on the Kalman filter algorithm ('Holmes' [12]), or, on the cellular automaton [13] ('CATS', [14]). Monte Carlo (MC) studies indicate quite similar performance of both algorithms: assuming single hit efficiencies of 96% and the nominal number of four interactions per event, i.e. about 80 tracks on average, reconstruction efficiencies between 91% and 96% are obtained for tracks with momenta larger than 1 GeV/c. The ghost rates, currently around 10%, will significantly decrease as soon as the information from the tracking systems downstream of the VDS becomes available.

During the past HERA-B commissioning periods [3], the VDS has been routinely used for target and beam diagnostics by analyzing the measured distributions of primary interaction vertices on the target wires. As an example, Fig. 5 shows an event with five well-separated interaction vertices, where each of them is defined by more than six tracks. The measured transverse and longitudinal vertex resolutions of about 80 μm and 600 μm, respectively, agree with MC predictions and are dominated by multiple scattering.

The successful integration of the VDS with the common HERA-B data acquisition and analysis system has been demonstrated by common data taking with VDS and two more HERA-B subdetectors, the electromagnetic calorimeter (ECAL) and the ring imaging Cherenkov detector (RICH). The resulting data has already made possible the reconstruction of those particles that emerge also from the 'golden' B^0 decay channel [4, p. 21]. Using the RICH as stand-alone tracker to estimate the momentum and requiring the VDS data two tracks and a vertex detached from the target wires, a clean

K_s^0 peak could be extracted; and by correlating tracks in the VDS with high-p_t clusters in the ECAL, a distinct J/Ψ signal in the invariant mass spectrum of e^+e^- pairs has been identified, which becomes even more pronounced if the RICH information is added.

In conclusion, the VDS is essentially complete, and it appears that its performance, including radiation tolerance, fulfils the requirements. The as yet uninstalled SL 8, located immediately after the VDS vessel, will be installed in March 2000. The commissioning of all other HERA-B subdetectors is expected to follow, so that first physics data taking can commence.

References

[1] E. Hartouni et al., HERA-B Design Report DESY-PRC 95/01, 1995.
[2] K.T. Knöpfle, Nucl. Instr. and Meth. A 368 (1995) 192.
[3] C. Bauer et al., Nucl. Instr. and Meth. A 418 (1998) 65.
[4] http://bellemac.kek.jp/INSTR99web/16Knoepfle.pdf or http://pluto.mpi-hd.mpg/~ktkno/conf_contributions.html.
[5] F. Klefenz, Diploma Thesis, Universität Heidelberg, 1997.
[6] I. Abt et al., Nucl. Instr. and Meth. A 439 (2000) 442.
[7] A. Bischoff et al., Nucl. Instr. and Meth. A 326 (1993) 27.
[8] V.M. Pugatch et al., Nuovo Cimento A 112 (1999) 1383.
[9] S. Brenner et al., Nucl. Instr. and Meth. A 339 (1994) 477 and 564.
[10] C. Bauer et al., CERN/LHCC/99-33 (1999) 508.
[11] U. Trunk, Ph.D. Thesis, Universität Heidelberg, 2000.
[12] M. Schmelling, HERA-B Internal Note 99-086, 1999.
[14] I. Kisel, S. Masciocchi, HERA-B Internal Note 99-242, 1999.
[13] I. Kisel et al., Nucl. Instr. and Meth. A 387 (1997) 433.